frontiers in Earth Science

ORIGINAL RESEARCH
published: 20 May 2021
doi: 10.3389/feart.2021.649011

Late Quaternary Kinematics and Deformation Rate of the Huoyanshan Structure Derived From Deformed River Terraces in the South Piedmont of the Eastern Chinese Tian Shan

Xue Yang[1,2], *Chuanyong Wu*[1,2]*, *Zhigang Li*[1,2]*, *Weitao Wang*[1,2], *Gan Chen*[1,2] *and Lei Duan*[1,2]

[1]Guangdong Provincial Key Lab of Geodynamics and Geohazards, School of Earth Sciences and Engineering, Sun Yat-sen University, Guangzhou, China, [2]Southern Marine Science and Engineering Guangdong Laboratory (Zhuhai), Zhuhai, China

OPEN ACCESS

Edited by:
Gang Rao,
Zhejiang University, China

Reviewed by:
Honghua Lu,
East China Normal University, China
Zhongtai He,
Ministry of Emergency Management, China
Qiang Xu,
Southwest Petroleum University, China

***Correspondence:**
Chuanyong Wu
cywueq@163.com
Zhigang Li
lizhigang@mail.sysu.edu.cn

Specialty section:
This article was submitted to Structural Geology and Tectonics, a section of the journal Frontiers in Earth Science

Received: 03 January 2021
Accepted: 03 May 2021
Published: 20 May 2021

Citation:
Yang X, Wu C, Li Z, Wang W, Chen G and Duan L (2021) Late Quaternary Kinematics and Deformation Rate of the Huoyanshan Structure Derived From Deformed River Terraces in the South Piedmont of the Eastern Chinese Tian Shan. Front. Earth Sci. 9:649011. doi: 10.3389/feart.2021.649011

The deformation pattern and strain partitioning in the Eastern Chinese Tian Shan are poorly known because of the lack of quantitative study of the kinematics and deformation rate of the major structure. Here we report a late Quaternary shortening rate for the most active reverse fault-and-fold in the Eastern Chinese Tian Shan. We quantified the kinematics and late Quaternary shortening rate of the Huoyanshan structure based on detailed high-resolution remote sensing image interpretations, field investigations and geological mapping. Six generations of folded terraces along the Tuyugou valley that showed the progressive folding process by the Huoyanshan structure were identified. A kinematic model of curved thrust fault propagation and folding allowed us to describe the terrace deformation pattern and subsurface fault geometry and calculate shortening across this structure. Combined with a regional age control of terrace T4 in the Tuyugou valley, a late Quaternary shortening rate of 2.0–3.2 mm/yr of the Huoyanshan structure was obtained. This is a relatively high shortening rate in the whole Eastern Chinese Tian Shan (roughly east of 88 E). This shortening rate of the Huoyanshan structure highlights that the ongoing India and Eurasia collision has affected the entire Tian Shan but shows two strain partitions: the main strain-absorption belt is located within the Eastern Chinese Tian Shan interior, but strain also occurs at the range-front foreland in the Western Tian Shan.

Keywords: Eastern Chinese Tian Shan, Huoyanshan structure, listric fault, shortening rate, strain partitioning

INTRODUCTION

To unravel the deformation across thrust-and-fold belts, various kinematic models that draw relationships between surface deformation, subsurface geometry and cumulative fault slip after the overlying strata were deposited have been proposed (Suppe, 1983; Erslev, 1991; Suppe et al., 1992; Medwedeff and Suppe, 1997; Suppe et al., 1997; Allmendinger and Shaw, 2000; Amos et al., 2007; Charreau et al., 2008; Le Béon et al., 2014; Saint-Carlier et al., 2016; Trexler et al., 2020; Wang et al., 2020b). Although strata, such as growth strata, are usually used as markers to depict fold kinematics and growth in previous studies Suppe et al. (1992), Storti and Poblet (1997), the difficulty of dating and lack of sediments limit the reconstruction of sequential kinematic development of thrust systems (Goode et al., 2011; Goode et al., 2014; Li et al., 2015; Stockmeyer et al., 2017; Wang et al., 2020b).

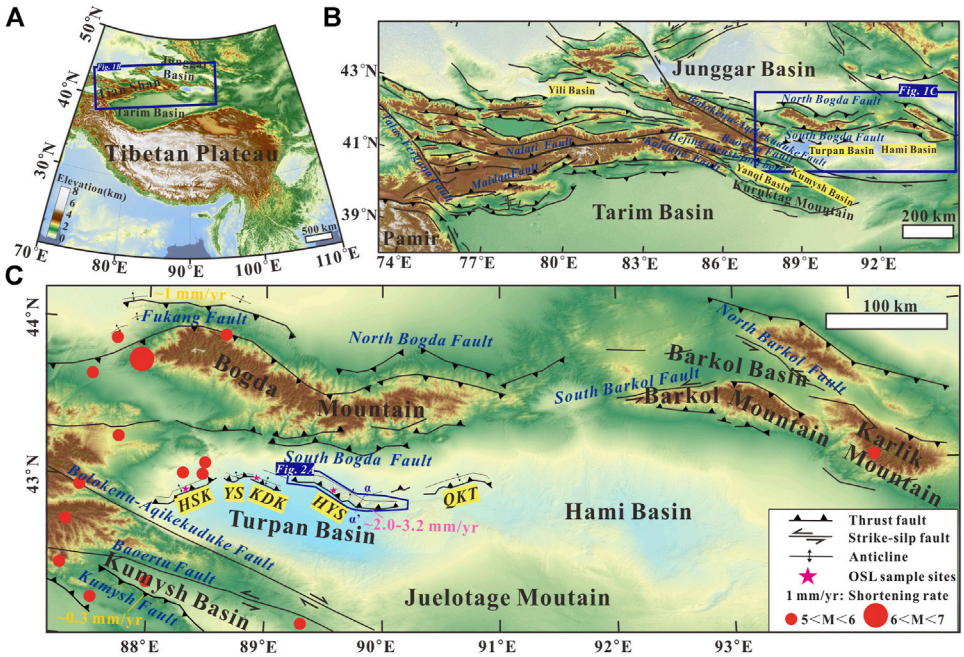

FIGURE 1 | (A) Topography of the Tibetan Plateau in response to the India-Eurasia collision. **(B)** Topography and major active faults in the Tian Shan (see **Figure 1A** for the location). **(C)** Topography and major active faults in the Eastern Chinese Tian Shan (see **Figure 1B** for the location). Fault data are from Deng et al., 2000; Shen et al., 2003; and Wu et al., 2016; red dots indicate earthquakes (M > 5) from 1900-01 to 2020-11 (downloaded from the United States Geological Survey at https://earthquake.usgs.gov/); shortening rates in yellow font in **Figure 1C** are from Wu et al., 2016 and Wang et al., 2020a; and those in pink font are from this study; HSK, Hongshankou structure; YS, Yanshan structure; KDK, Kendeke structure; HYS, Huoyanshan structure; QKT, Qiketai structure.

Commonly, even when growth strata have been preserved in outcrops, they are always missing across the core of a fold. In contrast, well-preserved abandoned fluvial terraces may extend across the entire fold and record incremental fold deformation. When combined with deformed river terraces and suitable kinematic models of fault-related folding Lavé and Avouac (2000), Thompson et al. (2002), Scharer et al. (2006), Hubert-Ferrari et al. (2007), Hu et al. (2015), Stockmeyer et al. (2017), Charreau et al. (2018), Cardozo and Oakley (2019), the spatial and temporal patterns of deformation of thrust-and-fold belts can be characterized.

In the Tian Shan, N-S crustal shortening dominates in response to the ongoing India-Eurasia collision during the late Cenozoic Tapponnier and Molnar (1979), Zhang et al. (2004), Yang et al. (2008), Zubovich et al. (2010), which has been accommodated by a series of roughly E-W-trending thrust-and-fold belts in foreland and/or intermontane basins ((**Figures 1A, B**; Avouac and Peltzer, 1993; Burchfiel et al., 1999; Deng et al., 2000; Thompson et al., 2002; Wu et al., 2016; Lu et al., 2019). Therefore, quantifying the geometry, kinematics and deformation rate of the thrust-and-fold belt is the key to exploring tectonic deformation and strain distribution in the Tian Shan region. Many studies e.g., Deng et al. (2000), Thompson et al. (2002), Shen et al. (2003), Hubert-Ferrari et al. (2007), Yang et al. (2008), Lu et al. (2019) have been conducted in the Western Tian Shan region to reveal the kinematics and deformation rate of fault-related folding and have shown that shortening is relatively uniformly distributed across the major intermontane basin boundaries and basin interior structures along a N-S transect of the Western Tian Shan, rather than solely at its margins. The Eastern Chinese Tian Shan is also dominated by intense tectonic deformation, which is shown by the study results of widespread active faults Deng et al. (2000), Lin et al. (2002), Wu et al. (2016), Huang et al. (2018a), Huang et al. (2018b), Ren et al. (2019), Wang et al. (2020a), paleoearthquake ruptures Feng (1997) and global positioning system (GPS) measurements (Zhang et al., 2004; Yang et al., 2008; Wang and Shen, 2020). However, in contrast to the Western Tian Shan, the deformation pattern and slip partitioning in the Eastern Chinese Tian Shan remain unclear because of the lack of quantitative study on the deformation rate and kinematics of the major structural belt.

The Huoyanshan (also known as Flame Mountain) structure, which is part of the Turpan foreland thrusting system (**Figures 1C**, **2A**), is the most active structural belt in the Eastern Chinese Tian Shan Deng et al. (2000) and consists of the Huoyanshan Fold and the Huoyanshan Fault (**Figure 2B**). A previous study Deng et al. (2000) determined the fault slip rate and further reconstructed the paleoseismic sequence based on the interpretation of trenches and dating of sediments. Kinematic models and shortening rates across the entire Huoyanshan structural belt have rarely been reported. This work aims to i) reveal the geometry of the Huoyanshan structure and estimate the late Quaternary crustal shortening rate from deformed river terraces and ii) understand the kinematics of this structure as well as strain partitioning in the Eastern Chinese Tian Shan.

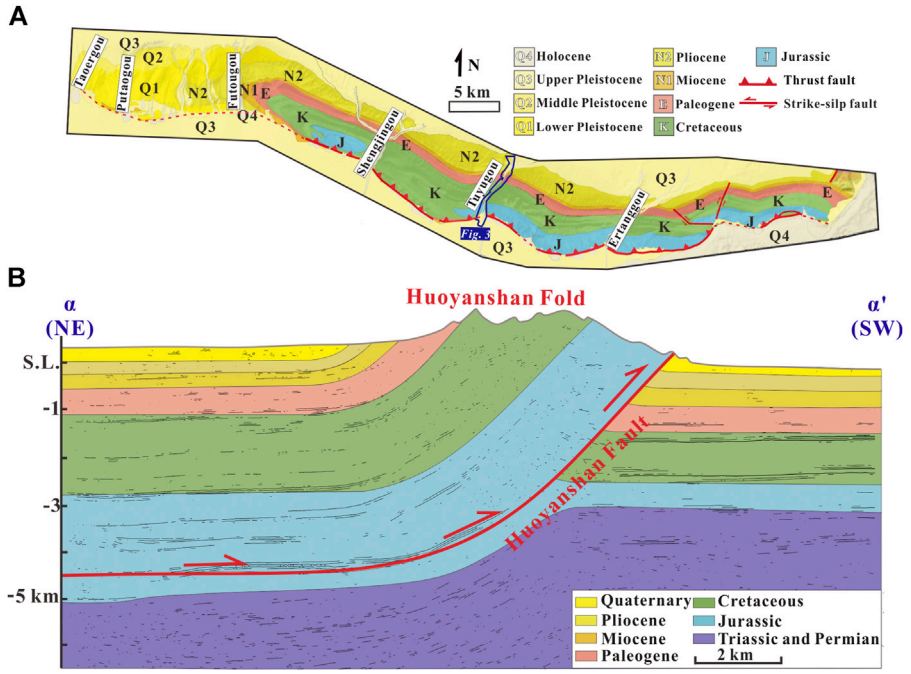

FIGURE 2 | (A) Simplified geologic map of the Huoyanshan structure (modified from Peng, 1995, see **Figure 1C** for the location) **(B)** Geologic cross-section α-α' (see **Figure 1C** for the location of α-α') of the Huoyanshan structure, interpreted from Deng et al., 2000; Yao et al., 2013; and Chang, 2016.

GEOLOGICAL SETTING

The Tian Shan orogenic belt, which is approximately 1,200 km north of the frontal Himalayan thrusts, is bounded by the Junggar Basin to the north and the Tarim Basin to the south and displays a basin-and-range topography (Tapponnier and Molnar, 1979; Burbank et al., 1999). GPS measurements and geological studies all suggest that the N-S convergence rate across the Tian Shan gradually decreases from west to east, with the shortening rate decreasing from ~12 mm/yr at 75 E Abdrakhmatov et al. (1996), Avouac and Peltzer (1993), Thompson et al. (2002), Zhang et al. (2004), Yang et al. (2008) to ~9 mm/yr at 78 E Campbell et al. (2019), and ~5 mm/yr of shortening occurs at 85 E (Wang and Shen, 2020). The Eastern Chinese Tian Shan is located to the east of 88 E longitude (**Figure 1B,C**). Although few large earthquakes have been recorded in its history, widespread active faults and present-day geodetic measurements attest to its active deformation. In the study region, the estimates of the N-S shortening rate across the whole range are based on present-day GPS measurements and range from 3 –5 mm/yr (Liang et al., 2013; Wang and Shen, 2020). The Eastern Chinese Tian Shan consists of the Bogda and Kuruktag ranges and several intermontane basins, such as the Turpan, Yanqi and Kumysh Basins (**Figure 1B**). Previous field investigations have recognized a series of active faults that bound the intermontane basins and accommodate N-S convergence (Deng et al., 2000; Lin et al., 2002; Fu et al., 2003; Wu et al., 2016; Wang et al., 2020a). The Eastern Chinese Tian Shan can be divided into two parts based on the Turpan basin (the largest intermontane basin). To the south of the Turpan Basin, the Bolokenu-Aqikekuduke Fault (BAF) and the Baoertu Fault (BETF) are strike-slip faults (Shen et al., 2003; Ren et al., 2019). Farther south, the Kuruktag range is thought to be dominated by right-lateral faulting since the late Cenozoic (Tapponnier and Molnar, 1979; Yin et al., 1998; Lin et al., 2002; Huang et al., 2018b). The right-lateral slip rate of the Kaiduhe Fault was estimated to be ~1.0 mm/yr Huang et al. (2018b), and the angle between these strike-slip fault trends and N-S shortening is small; hence, the crustal shortening accommodated by these faults is negligible. Moreover, a recent geological study reveals only ~0.3 mm/yr of shortening of the intermontane basin-bounding fault (Wang et al., 2020b), further indicating that crustal shortening is not prominent in the southern Turpan Basin. In contrast, the Bogda range to the north of the Turpan Basin has intense crustal shortening, as manifested by the strongly uplifted landscape. Based on surveying of the deformed late Quaternary alluvial fan and dating of the geomorphic surface, Wu et al. (2016) estimated ~1 mm/yr of shortening in the northern piedmont of the Bogda range. Within the Turpan Basin, the foreland thrusting system is composed of the Hongshankou, Yanshan, Kendeke, Huoyanshan, and Qiketai sub-belts from west to east (**Figure 1C**). These folds are the surface expressions of ramp thrusts whose decollement surface appears near the base of the Lower Jurassic sequence in the seismic profile (Deng et al., 1996; Deng et al., 2000; Yao et al., 2013). A series of inland rivers that originate from glaciers transversely cut the Turpan foreland thrusting system and flow into the Turpan Basin (**Figure 1C**), and river terraces are well developed in the thrusting system (Deng et al., 2000).

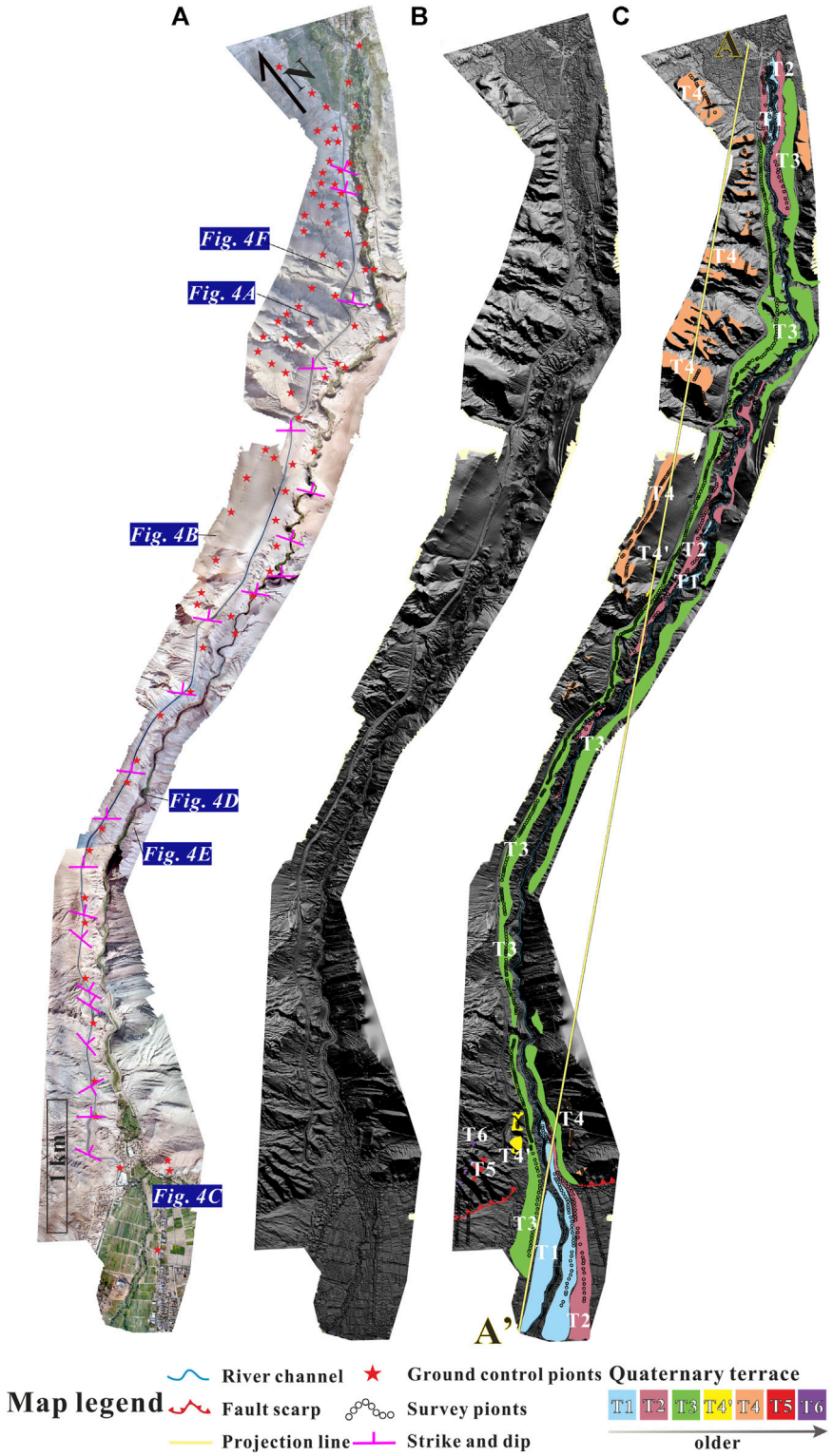

FIGURE 3 | (A) Orthography images of the Tuyugou Valley (see **Figure 2A** for the location). Red stars show the locations of GPS survey ground control points, and pink symbols indicate the locations and orientations of structural measurements. **(B)** Digital elevation model (DEM) surveyed by an unmanned aerial vehicle. **(C)** Geomorphic mapping of terraces in the Tuyugou Valley. Colours and numbers indicate the six generations of terraces (T4' represents a secondary terrace of T4), black dots show the individual points on terraces and river channels that are projected onto line A-A'.

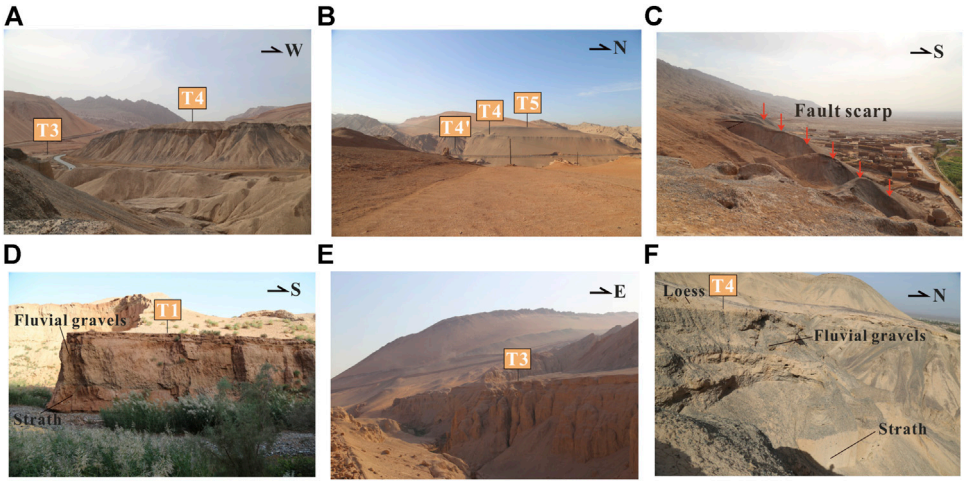

FIGURE 4 | (A), **(B)** Views W and N of the river terraces preserved in the Tuyugou Valley. **(C)** The location of the main E-W fault scarp is shown by red arrows. **(D)**, **(E)** and **(F)** Close-up views S, E, and N of the river terraces preserved in the Tuyugou Valley (for all locations, see **Figure 3A**).

Since the late Pleistocene, the Huoyanshan sub-belt is the largest active tectonic structure in the basin and is mainly composed of Jurassic to Cretaceous strata (**Figure 2A**). The structural pattern Peng (1995) suggests that it is an asymmetric fold that is dominated by a deep fault structure (**Figure 2B**). Jurassic, Cretaceous, Paleogene, Neogene strata, and the overlying late Quaternary alluvial terraces have been deformed by the fold (**Figure 2B**). A previous study indicated that the thrust located south of the Huoyanshan structure has a dip angle of ~30 (Deng et al., 2000). From west to east, several valleys cut through the Huoyanshan structure: the Taoergou, Putaogou, Futougou, Shengjingou, Tuyugou, and Ertanggou Valleys (**Figure 2A**). Among these valleys, the Tuyugou Valley, which cuts through the middle of the Huoyanshan structure, contains the most continuous terrace sequences.

MATERIALS AND METHODS

Classification and Age Constraints of Fluvial Geomorphology

In this study, we focused on the middle part of the Huoyanshan structure where it is crossed by the Tuyugou Valley. Terrace classification and mapping were conducted based on Google Earth image interpretation and field investigations. Terraces of the Tuyugou Valley were interpreted again with a high-resolution digital elevation model (DEM). To obtain the high-resolution DEM of the Tuyugou Valley, 4,782 photos were captured by an unmanned aerial vehicle (UAV). To improve the accuracy and precision of the DEM, 85 ground control points (**Figure 3A**) that cover all surveying areas were placed and measured with a real-time kinematic global positioning system (RTK-GPS). The DEM was derived using PhotoScan (version 1.26.2834) based on the classical workflow (Agisoft L.L.C., 2018): 1) loading the 4,782 photos of the Tuyugou Valley acquired by the aerial platform into PhotoScan, then inspecting the loaded images and removing unnecessary images (after the removing procedure, 4,600 photos remain); 2) aligning these photos; 3) building a dense point cloud; 4) building a mesh (3D polygonal model); 5) generating a texture; 6) building a tiled model; 7) georeferencing 85 RTK-GPS surveyed ground control points that are distributed on the terrace surfaces; 8) repeating steps 1–6; and 9) building the DEM (**Figures 3B, C**).

Due to coarse-grained material and the low quartz content in the sediments, it is difficult to collect appropriate samples for dating from river terraces in the Tuyugou Valley (**Figures 4A, B, D, E, F**). Although the exact number of terraces within each division may vary locally, several regional terraces could be correlated with regional climate change. In this study, terrace ages rely on previous studies of the neighbouring valley (Peng, 1995; Deng et al., 2000). Terraces that cross the anticline may be divided into tectonic and climatic terraces. The climatic terraces are more widely developed, are relatively continuous compared to tectonic terraces, and can be compared regionally. The Turpan Basin, which is located in the hinterland of Eurasia and lying in the northeastern part of the Tian Shan, has a semiarid climate. The Quaternary denudation and sedimentation process, in terms of erosion and deposition, was inevitably affected by the impact of glaciation (glacial and interglacial periods) and climate change. Quaternary sediments filling the basin and geomorphological units such as river terraces have been affected by climate change. The river terraces in the Turpan Basin are mainly distributed in the river valleys of the Turpan foreland thrusting system, which can be compared and correlated locally.

The Turpan foreland thrusting system (**Figure 1C**) contains a widely developed generation of terraces. These terraces are mainly composed of early late Pleistocene fluvial sediments with thicknesses of 5–10 m and form a relatively broad platform on the tops of the mountains in the Turpan foreland thrusting system, including the western Hongshankou mountaintop, western Kendeke mountaintop, and Huoyanshan mountaintop Deng et al. (2000), Peng (1995), which indicates

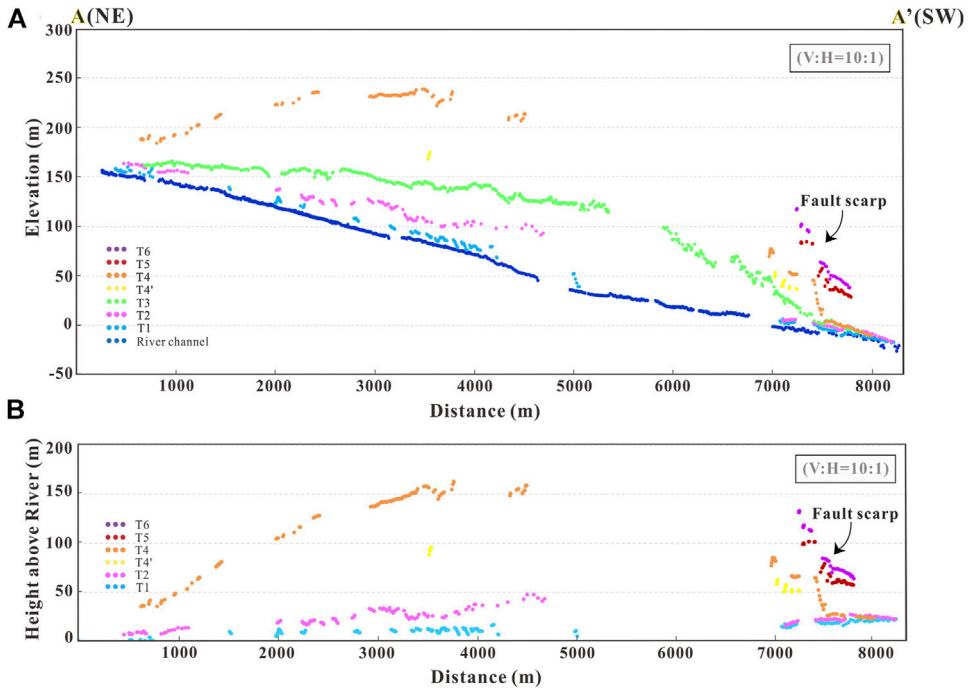

FIGURE 5 | (A) Terraces and river channel longitudinal profiles across the Huoyanshan structure showing the pattern and amounts of deformation of different terraces. **(B)** Relative heights of the terraces to the modern river channel; a polynomial that fits the modern riverbed is subtracted from each fluvial terrace to eliminate the modern river gradient. The vertical exaggeration is 10. The distance is projected along line A-A', where A' is the direction downstream, and a fault scarp exists at the southern margin of the Tuyugou valley (see **Figure 3C** for the location).

that this generation of terraces is climatic. The heights above the river of the main portions of this generation of terraces are ~90 m on the Hongshankou mountaintop, ~100 m on the Kendeke mountaintop, ~100 m in Putaogou Valley in the Huoyanshan structure, and ~100 m in Shengjingou Valley in the Huoyanshan Mountains (**Figures 1C**, **2A**; Peng, 1995). The optically stimulated luminescence (OSL) ages of this terrace have been dated in previous studies: on the Hongshankou mountaintop, 56.9 ± 4.4 ka (Deng et al., 2000); on the Kendeke mountaintop, 73.8 ± 5.8 ka Peng (1995); and on the southeast mountaintop of the Shengjingou Valley, 61.2 ± 11.6 ka (Deng et al., 2000). The abandonment age of this terrace seems to be related to the climatic event of early Last Glacial during 55–75 ka, corresponding to MIS 4 (Deng et al., 2000; Wu et al., 2004).

In the Tuyugou Valley, T4 is a major terrace that is developed on the mountaintop of the Huoyanshan structure and is relatively broad and continuous (**Figure 4B**). The maximum height above river of T4 is ~160 m (considering that the Tuyugou Valley is in the middle of the Huoyanshan structure, the deformation is much more intense). The terrace is composed of ~10 m of fluvial sediments. By comparing the geomorphic characteristics of T4 in the Tuyugou Valley and the terrace described above, T4 could be compared with the widely developed terrace in the Turpan foreland thrusting system. Therefore, the age of T4 in the Tuyugou Valley was constrained by the ages have been dated that is 56.9 ± 4.4–73.8 ± 5.8 ka. These ages were defined by OSL samples that had been taken from fine sand in the middle of fluvial deposits (**Figure 1C**; Peng, 1995; Deng et al., 2000).

Determination of Crustal Shortening by Morphometry

To determine the pattern and amount of deformation in the Huoyanshan structure, topographic lines were plotted at terrace surfaces and modern riverbeds (**Figure 3C**), and the coordinates and elevations of the topographic lines were extracted from the DEM, which was derived from UAV measurements (these procedures were conducted in ArcMap, version 10.8). Then, these raw survey measurements of the topographic lines were projected onto the N-S-trending line A-A' (**Figure 3C**), parallel to the Tuyugou Valley and roughly perpendicular to the trend of the synclinal axial surface. To depict the spatial distribution geometry of terraces and riverbeds, topographic profiles along all terraces and the modern riverbed were plotted (**Figure 5A**). To eliminate the modern river gradient, a polynomial that fits the modern riverbed was subtracted from each fluvial terrace (**Figure 5B**). The undeformed and maximum terrace heights were calculated based on the data reflected in **Figure 5B** (all with errors of 1 σ). To eliminate the terrace height caused by river incision (base level changes in

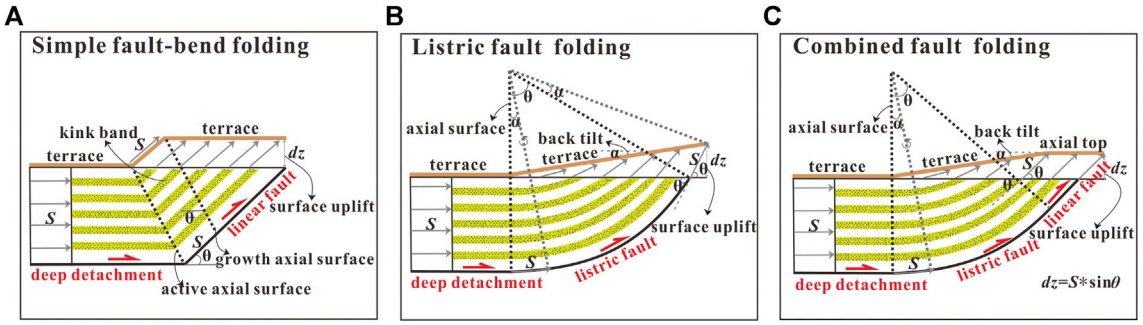

FIGURE 6 | Kinematic models of different reverse fault-related folds. **(A)** Simple fault-bend folding (modified from Suppe, 1983; Suppe et al., 1992, Suppe et al., 1997; Erslev, 1991; Medwedeff and Suppe, 1997): the fault grows linearly, the surface deformation is uniform within each dip domain defined by a planar fault, and the backlimb is short and relatively steep. **(B)** Listric fault folding (modified from Amos et al., 2007; Charreau et al., 2008): the fault grows listrically by limb rotation, the surface deformation is sequential and nonuniform, and the backlimb is long and flatter with no axial top. **(C)** Combined fault folding (modified from wang et al., 2020b, Trexler et al., 2020): the fault grows listrically and then connects to a linear segment and dips at a constant angle to the surface. The surface deformation is similar to the listric fault but with an axial top. (In all three models, we assume there is no tilt in the substrata while the surface above the fault is undeformed, and the deep fault is initially developed from a subhorizontal detachment structure.)

TABLE 1 | Terrace deformation and kinematic model inputs and results.

Terrace	Deformed height (1σ)	Undeformed height (1σ)	Surface uplift (max-min)	Horizontal shortening (max-min)	Age of terrace (1σ)	Horizontal slip rate (max-min)
T1	16.6 ± 0.3 m	0.9 ± 0.6 m	14.8–16.6 m	19.3–21.7 m	/	/
T2	45.7 ± 1.8 m	7.1 ± 0.1 m	36.7–40.5 m	47.9–52.9 m	/	/
T4	161.6 ± 1.4 m	36.9 ± 1.1 m	122.2–127.2 m	159.5–166.1 m	56.9 ± 4.4–73.8 ± 5.8 ka Peng (1995); Deng et al. (2000)	2.0–3.2 mm/yr

landscapes can cause river incision) and obtain vertical uplifts that have been caused by only fold growth, we used the maximum terrace height minus the undeformed terrace height. Crustal shortening was calculated through the trigonometric relationship in the kinematic model (**Figures 6A, B, C**), and the uncertainty was mainly derived from the terrace age and crustal shortening (**Table 1**). To reflect the degrees of terrace deformation, the tilted angles of the backlimbs and forelimbs were calculated through the trigonometric relationships between the horizontal lengths of the backlimbs and forelimbs and the vertical uplift of each terrace (**Figure 7A**).

Structural Analysis

To construct the kinematic model of the Huoyanshan structure, 22 bedding attitudes of bedrock at intervals of ~300–400 m (the measurement interval increased as the bedrock outcrops improved) were measured across the Tuyugou Valley (**Figures 3A**, **7B**). By integrating the vertical uplift longitudinal profile of terraces (**Figure 5B**), the measured bedding attitudes and the combined fault folding model (**Figure 6C**), the best-fit kinematic model between the Quaternary terrace surface deformation and the inferred subsurface geometry in the Huoyanshan structure was established. Because high-resolution seismic profiles were not available across the Tuyugou Valley, the depth of the decollement (**Figure 7B**) was constrained and inferred from previously published nearby seismic reflection data (**Figure 2B**; Deng et al., 2000; Yao et al., 2013; Chang, 2016).

RESULTS

Terrace Description and Deformation

Six terraces along the Tuyugou Valley, T1–T6, that increase in height above the modern riverbed, were defined. (**Figure 3C**). Most of these terraces are strath terraces that have been eroded into the base rock, capped and covered by several metres of fluvial gravels and subsequently buried by variable depths of eolian loess (**Figures 4D**, F). T4 is the most spatially extensive and best-preserved terrace, and it has a secondary terrace, namely, T4' (**Figure 3C**). Among these terraces, only T3 is capped by 50–80 m of lacustrine deposits, which are dominated by grey mudstone, green mudstone and red siltstone and are horizontally bedded (**Figure 4E**). The presence of lacustrine deposits indicates that there was a relatively humid environment during the T3 formation period. The width of the Tuyugou Valley is relatively narrow (**Figures 3A**, **4E**), which could cause sediments to be dammed in the river and create a lake.

Terraces preserved in the western Tuyugou Valley are more continuous (**Figure 3C**). T6–T5 are not very continuous compared with other terraces and have been found only at the southern margin of the valley (~7–8 km in **Figure 5A**). Different

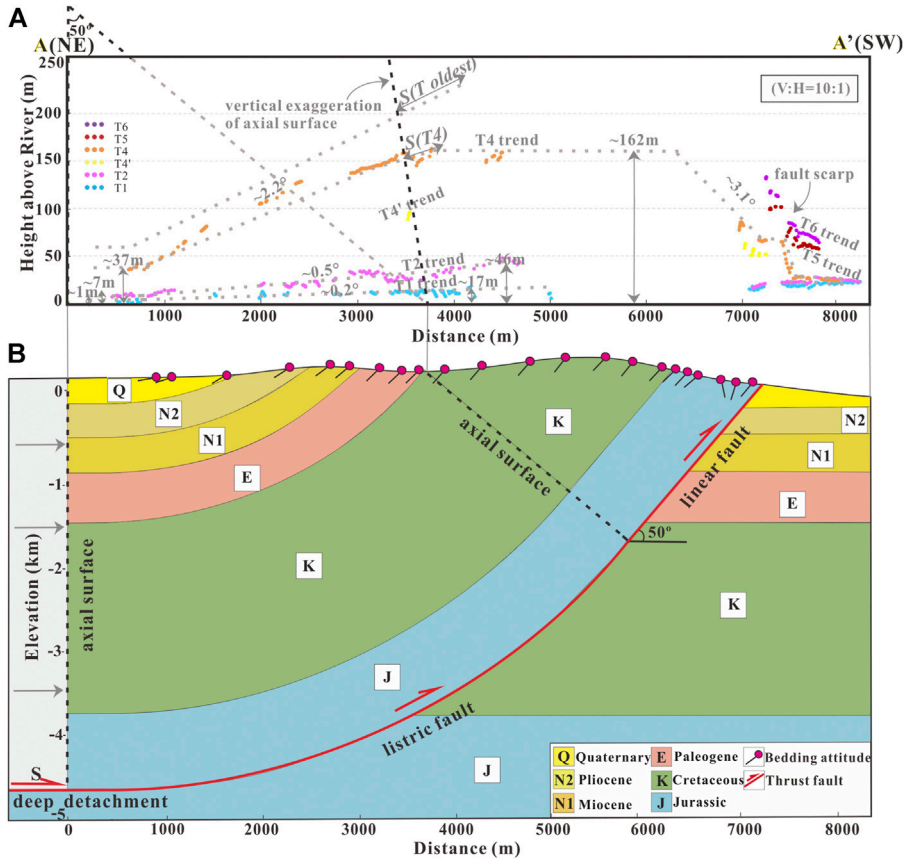

FIGURE 7 | According to the terrace deformation pattern and bedding attitudes, we use the combined fault folding model (see **Figure 6C** for detailed information) to reconstruct the kinematic relationship between the deformed river terraces and the subsurface fault geometry. **(A)** Terrace deformation pattern of the Tuyugou Valley (see **Figure 3C** for the location of A-A'). **(B)** Subsurface fault geometry at the Tuyugou Valley, which is inferred from the terrace deformation pattern, bedding attitudes and the combined fault folding model.

degrees of deformation exist in all terraces. Compared with the younger terraces, such as T2 and T1, the older terraces have deformed much more significantly. T6-T4 have been significantly deformed by the Huoyanshan Fault (**Figure 5A**). These terraces reach their peak heights at the core of the anticline and gradually extend to the wings (~4–6 km in **Figure 5A**). T3 appears to be nearly horizontal in the true elevation profile in **Figure 5A**. We assume that T3 was deposited by the sediment dammed in the river during the formation of the lake. Regardless of the origin of the terraces in the Tuyugou Valley, the terrace surfaces could be deformed by folding. However, due to its lacustrine deposit characteristics, there is no reason to believe that T3 was graded by the river compared with other fluvial terraces; therefore, T3 was not used to restore the kinematics of folding.

The Huoyanshan Fold has a relatively short forelimb that is approximately 1.4 km long. After ~8 km, terraces and modern riverbeds meet on undeformed alluvial fans. The length of the axial top is ~2.5 km at T4 (the discontinuous terrace makes it difficult to confirm). The backlimb is relatively long (~3.0 km), and the anticline has a relatively broad wavelength (~7 km) (**Figure 5B**). The vertical uplifts (relative to the undeformed terrace surface) are 14.8–16.6 m for T1, 36.7–40.5 m for T2, and 122.2–127.2 m for T4 (**Table 1**). The tilt angles of deformed terraces increase with terrace age; they are 0.2° for T1, 0.5° for T2, and 2.2° for T4. These characteristics demonstrate that fluvial terraces in the Tuyugou Valley are syntectonic sediments deposited during the growth of the fold that recorded the folding deformation process, and the older terraces accumulated more fold deformations than the younger terraces.

Kinematic Model and Late Quaternary Slip Along the Huoyanshan Reverse Fault-and-fold Belt

The most important aspect of calculating the deformation rate of the Huoyanshan structure is establishing the kinematic relationship between terrace deformation and subsurface geometry. We have summarized several kinematic models to reflect different thrust fault-related folding processes (Suppe, 1983; Erslev, 1991; Suppe et al., 1992; Medwedeff and Suppe, 1997; Suppe et al., 1997; Allmendinger, 1998; Amos et al., 2007; Charreau et al., 2008; Trexler et al., 2020; Wang et al., 2020b). In the simple fault-bend folding model, the fault grows linearly, the surface deformation is uniform within each dip domain defined

by the planar fault, and the backlimb is short and relatively steep (**Figure 6A**). In listric fault folding model, the fault grows listrically by limb rotation, the surface deformation and dip angles of the bedrock are sequential and nonuniform, the backlimb is long and has a gentler dip, and no axial top exists (**Figure 6B**). In the combined fault folding model, the fault grows listrically and then connects to a linear segment and follows a constant dip angle to the surface. The surface deformation pattern is similar to the listric fault model but with an axial top (**Figure 6C**). In all three models, it is assumed that there was no tilt in the substrata when the surface above the fault was undeformed, and the deep fault was initially developed from a subhorizontal detachment structure.

Bedding attitude data along the Tuyugou Valley indicate forelimb dips reaching 70° and gentler backlimb dips from ~50 to 12 with a northeast dip direction. Between the forelimb and the backlimb, the dip domain is ~50 (**Figure 7B**). The dip angle of each fold segment and the characteristics of terrace deformation in *Terrace Description and Deformation* reveal that the terrace deformation pattern and subsurface structure are incompatible with other fault-related folding models except for the combined fault folding model (**Figure 6C**). Therefore, we interpret the Huoyanshan fault as a fault that dips 50, is a planar feature that extends from the surface to ~2 km depth and connects to a listric segment that gradually merges into the detachment and changes its dip angle to 0 at ~4.0–5.0 km depth (**Figure 7B**).

Total shortening was estimated from the trigonometric relationship between the vertical uplift of the terrace and the dip angle of the bedrock at the surface (Trexler et al., 2020). If folding results from total horizontal shortening S that detaches from the footwall with a vertical surface uplift of dz and a surface dip angle θ, the relationship between these parameters is:

$$s = \frac{dz}{\sin\theta}$$

Following this approach and using the dip angle of the fault plane as 50, the different vertical uplifts of the terraces yield shortening values of 19.3–21.7 m for T1, 47.9–52.9 m for T2, and 159.5–166.1 m for T4. The shortening rate of T4 is 2.0–3.2 mm/yr after T4 was abandoned. The uncertainty in the shortening rate is mainly derived from the uncertainties in the length of shortening and the age of the terrace (**Table 1**). As the surface of T4 is not continuous and given the orientation of the surface, T4 would reach even higher above the river channel (**Figure 5B**), which indicates that the shortening estimate is a minimum (**Figure 6C**). The terrace age of T4 is defined by OSL, samples for which were taken from fine sand in the middle of fluvial deposits Peng (1995), Deng et al. (2000); therefore, the OSL age is a maximum estimate of the terrace abandonment age considering erosion, which may cause the actual terrace abandonment age to be younger. Based on these two factors, the estimate of the shortening rate is the minimum value.

DISCUSSION

Fault Geometry

We used the combined fault folding model (**Figure 6C**) to reconstruct the geometric features of terrace deformation and subsurface fault geometry and believe that it is the best-fit kinematic model of the Huoyanshan structure. In this model of the Huoyanshan structure in the Tuyugou Valley, the subsurface fault starts with a subhorizontal detachment and is connected by a listric segment to a linearly dipping fault. As mentioned above in *Terrace Description and Deformation*, it is difficult to confirm the existence of an anticline axial top because the T4 surface is not continuous, which makes it difficult to identify. However, if there is no axial top, the fault follows the simple listric folding model (**Figure 6B**), and the dip angle of the bedrock should gradually change at the surface, which is not consistent with our measurement results of the bedding attitudes across the fold. According to these measurement results, a dip domain is present after the dip angle of bedrock reaches ~50 (**Figure 7B**). The appearance of the dip domain indicates the existence of a linear fault segment that forms an axial top at the surface. Integration of available subsurface data lends validation to this interpretation. The subsurface fault geometry inferred in this study is consistent with the characteristics reflected in the interpreted cross-section (**Figures 2B**, **7B**).

In addition, according to the interpretation, the fault crosses the main fault and forms a fault scarp. However, there is a good chance of the development of a secondary fault that outcrops at the surface, as intense deformation exists in front of the forelimb (**Figure 7B**). It is commonly a challenge to differentiate among kinematic models for specific thrust fault-related folds and match the geometry of subsurface faults with the patterns of deformed surfaces. This requires both surface deformation patterns and high-resolution seismic reflection data of the subsurface fault to determine which type of model most represents the nature of faulting and folding (Goode et al., 2011; Goode et al., 2014; Li et al., 2015; Stockmeyer et al., 2017; Wang et al., 2020b). To improve our work, a detailed study of the entire Huoyanshan structure should be carried out, such as investigating terrace deformation in other valleys of the Huoyashan area and constraining the subsurface fault geometry with a high-resolution seismic profile.

Slip-Partitioning in the Eastern Chinese Tian Shan

This study infers a crustal shortening rate of 2.0–3.2 mm/yr across the Huoyanshan structure since the late Quaternary, which is significantly larger than that across the other intermontane basin-bounding faults in this region. Within the Yanqi Basin in the Eastern Chinese Tian Shan, by using seismic data and the attitude of strata and faults to restore the geometry of the fold, Li et al. (2012) calculated the shortening rate in the Hejing thrust-fold belt, which has been ~0.3 mm/yr since the late Pleistocene. By studying the typical offset landforms and lineaments of scarps on the eastern segment of the north-edge fault of the Yanqi Basin, Huang et al. (2018a) constrained the shortening rate to 0.4–0.5 mm/yr on the northern margin of the basin. Based on dating the alluvial fan surfaces, measuring the heights of the fault scarps, and investigating a paleoearthquake trench wall, Wang et al. (2020a) estimated that a ~0.3 mm/yr shortening rate was accommodated by the Kumysh Fault during the late Quaternary. The shortening rate was estimated to be ~1 mm/yr since the late Quaternary at the

Bogda foreland thrust fault through geologic and geomorphologic field surveys, trench excavation and OSL dating (Wu et al., 2016). The relatively high shortening rate of the Huoyanshan structure indicates that it is the main strain-absorption belt in the Eastern Chinese Tian Shan region. In the Western Tian Shan (**Figure 1B**), the strain was proposed as mainly being partitioned into the foreland thrusting system Yang et al. (2008) or evenly distributed across the entire mountain (Thompson et al., 2002), rather than solely at its margins. What mechanism could explain the relatively large crustal shortening rate of the Huoyanshan structure in the Eastern Chinese Tian Shan?

The Turpan basin is underlain by a strong basement Allen et al. (1993) and extends approximately 100 km in the N-S direction. Petroleum seismic profiles and our field mapping indicate that the folds in the northern Turpan Basin mainly involved Mesozoic and Cenozoic sedimentary rocks (Deng et al., 2000). If the pre-Mesozoic basement of the Turfan Basin did not deform, the thin-skinned structure belt would have splayed from the basin-bounding fault at the margin of the basin. With the foreland-ward expansion of the range, the stress was concentrated on the thrust faults in the northern margin of the Turpan Basin. Active deformation propagated into the Huoyanshan structure belt. Therefore, high crustal shortening rate can be observed within the intermontane basin (Campbell et al., 2019). The Huoyanshan thrust fault-and-fold belt may have acted to concentrate stress onto the Turpan Basin margin fault in the north, which, in turn, may have built up the present-day high-elevation Bogda range observed today (**Figure 1C**). The rigid blocks in an orogenic belt are always the places where major crustal shortening and deformation occur and determine the deformation pattern.

CONCLUSION

Based on detailed high-resolution remote sensing image interpretations, field investigations and geological mapping of the Huoyanshan structure, we quantify the kinematics and late Quaternary shortening rate of the Huoyanshan structure, and we summarize the following conclusions.

By considering both the bedrock structure recorded by folded strata and the terrace deformation pattern, we propose a kinematic model of curved thrust fault propagation folding that describes the whole structural deformation of the Huoyanshan structure.

Based on the unique kinematic model, the survey of the deformed river terraces, and age correlation, we estimate a late Quaternary shortening rate of 2.0–3.2 mm/yr for the structure.

Comparisons of strain are partitioned along several structures within the Western Tian Shan, and our shortening rate of the Huoyanshan structure highlights that the main strain-absorption belt is located within the Eastern Chinese Tian Shan interior.

DATA AVAILABILITY STATEMENT

The original contributions presented in the study are included in the article/Supplementary Material, further inquiries can be directed to the corresponding authors.

AUTHOR CONTRIBUTIONS

ZL, CW, and XY initiated the study. CW, ZL, WW, and XY designed the manuscript, XY carried out the calculation and interpretation work and wrote the manuscript. CW, ZL, and WW provided helpful discussions and helped to improve the manuscript. Co-authors GC, LD helped to carried out filed work.

FUNDING

This research was supported by Natural Science Foundation of China (41672208, 41772209, 42030301), Operation Expenses for Universities' Basic Scientific Research of Sun Yat-sen University (19lgpy60), and The Second Tibetan Plateau Scientific Expedition and Research Program (STEP) (2019QZKK0901).

ACKNOWLEDGMENTS

We thank the reviewers for their constructive comments, which significantly improved the manuscript, and the editor for editorial handling of the paper.

REFERENCES

Abdrakhmatov, K. Y., Aldazhanov, S. A., Hager, B. H., Hamburger, M. W., Herring, T. A., Kalabaev, K. B., et al. (1996). Relatively Recent Construction of the Tien Shan Inferred from GPS Measurements Crustal Deformation Rates. *Nature* 384, 450–453.

Agisoft L. L. C. (2018). Agisoft PhotoScan User Manual Professional Edition Version 1.4. Available at: https://www.agisoft.com/pdf/photoscan-pro_1_4_en.pdf (Accessed September 19, 2020).

Allen, M. B., Windley, B. F., and Chi, Z. (1993). Paleozoic Collisional Tectonics and Magmatism of the Chinese Tien-Shan, Central Asia. *Tectonophysics* 220, 89–115. doi:10.1016/0040-1951(93)90225-9

Allmendinger, R. W. (1998). Inverse and Forward Numerical Modeling of Trishear Fault-Propagation Folds. *Tectonics* 17, 640–656. doi:10.1029/98tc01907

Allmendinger, R. W., and Shaw, J. H. (2000). Estimation of Fault Propagation Distance from Fold Shape: Implications for Earthquake Hazard Assessment. *Geology* 28, 1099. doi:10.1130/0091-7613(2000)282.0.CO;2

Amos, C. B., Burbank, D. W., Nobes, D. C., and Read, S. A. L. (2007). Geomorphic Constraints on Listric Thrust Faulting: Implications for Active Deformation in the Mackenzie Basin, South Island, New Zealand. *J. Geophys. Res.* 112, B03S11. doi:10.1029/2006JB004291

Avouac, J. P., and Peltzer, G. (1993). Active Tectonics in Southern Xinjiang, China: Analysis of Terrace Riser and Normal Fault Scarp Degradation along the Hotan-Qira Fault System. *J. Geophys. Res.* 98, 21773–21807. doi:10.1029/93jb02172

Burbank, D. W., McLean, J. K., Bullen, M., Abdrakhmatov, K. Y., and Miller, M. M. (1999). Partitioning of Intermontane Basins by Thrust-related Folding, Tien Shan, Kyrgyzstan. *Basin Res.* 11, 75–92. doi:10.1046/j.1365-2117.1999.00086.x

Burchfiel, B. C., Brown, E. T., Qidong, D., Xianyue, F., Jun, L., Molnar, P., et al. (1999). Crustal Shortening on the Margins of the Tien Shan, Xinjiang, China. *Int. Geology. Rev.* 41, 665–700. doi:10.1080/00206819909465164

Campbell, G. E., Walker, R. T., Abdrakhmatov, K., Carolin, S., Carr, A. S., Elliott, J. R., et al. (2019). Rapid Late Quaternary Slip, Repeated Prehistoric Earthquake Rupture, and Widespread Landsliding Associated with the Karakudzhur Thrust, Central Kyrgyz Tien Shan. *Tectonics* 38, 3740–3764. doi:10.1029/2018TC005433

Cardozo, N., and Oakley, D. (2019). Inverse Modeling for Possible rather Than Unique Solutions. *J. Struct. Geology.* 125, 285–295. doi:10.1016/j.jsg.2018.05.026

Chang, Q. L. (2016). Mapping Method of Pre-stack Depth Migration Technique of Huoyanshan Structure in Turpan-Hami Basin. [Chengdu (Sichuan)]: Southwest Petroleum University. [master's thesis] [in Chinese with English abstract].

Charreau, J., Avouac, J. P., Chen, Y., Dominguez, S., and Gilder., S. (2008). Miocene to Present Kinematics of Fault-Bend Folding across the Huerguosi Anticline, Northern Tianshan (China), Derived from Structural, Seismic, and Magnetostratigraphic Data. *Geology* 36, 871–874. doi:10.1130/G25073A.1

Charreau, J., Saint-Carlier, D., Lavé, J., Dominguez, S., Blard, P. H., Avouac, J. P., et al. (2018). Late Pleistocene Acceleration of Deformation across the Northern Tianshan Piedmont (China) Evidenced from the Morpho-Tectonic Evolution of the Dushanzi Anticline. *Tectonophysics* 730, 132–140. doi:10.1016/j.tecto.2018.02.016

Deng, Q., Feng, X., Zhang, P., Xu, X., Yang, X., Peng, S., et al. (2000). *Active Teconics in Tianshan*. Beijing: Seismological Press [in Chinese with English abstract].

Deng, Q., Zhang, P., Xu, X., Yang, X., Peng, S., and Feng, X. (1996). Paleoseismology in the Northern Piedmont of Tianshan Mountains, Northwestern China. *J. Geophys. Res.* 101, 5895–5920. doi:10.1029/95JB02739

Erslev, E. A. (1991). Trishear Fault-Propagation Folding. *Geology* 19, 617–620. doi:10.1130/0091-7613(1991)019<0617:tfpf>2.3.co;2

Feng, X. (1997). *Paleoseismology in Xinjiang*. Xinjiang: Health science and technology publishing house, 1–260. [in Chinese with English abstract].

Fu, B., Lin, A., Ken-ichi, K., Tadashi, M., and Guo, J. (2003). Quaternary Folding of the Eastern Tian Shan, Northwest China. *Tectonophysics* 369, 79–101. doi:10.1016/S0040-1951(03)00137-9

Goode, J. K., Burbank, D. W., and Bookhagen, B. (2011). Basin Width Control of Faulting in the Naryn Basin, South-central Kyrgyzstan. *Tectonics* 30, TC6009. doi:10.1029/2011TC002910

Goode, J. K., Burbank, D. W., and Ormukov, C. (2014). Pliocene-Pleistocene Initiation, Style, and Sequencing of Deformation in the Central Tien Shan. *Tectonics* 33, 464–484. doi:10.1002/2013TC003394

Hu, X., Pan, B., Kirby, E., Gao, H., Hu, Z., Cao, B., et al. (2015). Rates and Kinematics of Activeshortening along the Eastern Qilian Shan, China, Inferred from Deformed Fluvial Terraces. *Tectonics* 34, 2478–2493. doi:10.1002/2015TC003978

Huang, W., Yang, X., Li, S., and Yang, H. (2018a). Holocene Slip Rate and Earthquake Hazard of the North-edge Fault of the Yanqi Basin, Southeastern Tian Shan, China. *Seismology Geology.* 40, 186–203. [in Chinese with English abstract]. doi:10.3969/j.issn.0253-4967.2018.01.014

Huang, W., Yang, X., Li, S., and Yang, H. (2018b). The Late Quaternary Activity Characteristics of the Strike-Slip Faults in the Tianshan Orogenic Belt: A Case Study of Kaiduhe Fault. *Seismology Geology.* 40, 1040–1058. [in Chinese with English abstract]. doi:10.3969/j.issn.0253-4967.2018.05.006

Hubert-Ferrari, A., Suppe, J., Gonzalez-Mieres, R., and Wang, X. (2007). Mechanisms of Active Folding of the Landscape (Southern Tian Shan, China). *J. Geophys. Res.* 112, B03S09. doi:10.1029/2006JB004362

Lavé, J., and Avouac, J. P. (2000). Active Folding of Fluvial Terraces across the Siwaliks Hills, Himalayas of Central Nepal. *J. Geophys. Res.* 105, 5735–5770. doi:10.1029/1999jb900292

Le Béon, M., Suppe, J., Jaiswal, M. K., Chen, Y. G., and Ustaszewski, M. E. (2014). Deciphering Cumulative Fault Slip Vectors from Fold Scarps: Relationships between Long-Term and Coseismic Deformations in Central Western Taiwan. *J. Geophys. Res. Solid Earth* 119, 5943–5978. doi:10.1002/2013JB010794

Li, A., Yang, X., Huang, W., and Yiliyaer (2012). Quaternary Deformation of the Hejing Thrust-fold Belt on Northern Margin of the Yanqi Basin, Southern Tianshan. *Seismology Geology*. 34, 240–253. [in Chinese with English abstract]. doi:10.3969/j.issn.0253-4967.2012.02.004

Li, T., Chen, J., Thompson, J. A., Burbank, D. W., and Yang, H. (2015). Hinge-migrated Fold-scarp Model Based on an Analysis of Bed Geometry: A Study from the Mingyaole Anticline, Southern Foreland of Chinese Tian Shan. *J. Geophys. Res. Solid Earth* 120, 6592–6613. doi:10.1002/2015JB012102

Liang, S., Gan, W., Shen, C., Xiao, G., Liu, J., Chen, W., et al. (2013). Three-dimensional Velocity Field of Present-Day Crustal Motionof the Tibetan Plateau Derived from GPS Measurements. *J. Geophys. Res. Solid Earth* 118, 5722–5732. doi:10.1002/2013JB010503

Lin, A., Fu, B., Kano, K. I., Maruyama, T., and Guo, J. (2002). Late Quaternary Right-lateral Displacement along Active Faults in the Yanqi Basin, Southeastern Tian Shan, Northwest China. *Tectonophysics* 354, 157–178. doi:10.1016/S00401951(02)00288-3

Lu, H., Li, B., Wu, D., Zhao, J., Zheng, X., Xiong, J., et al. (2019). Spatiotemporal Patterns of the Late Quaternary Deformation across the Northern Chinese Tian Shan Foreland. *Earth-Science Rev.* 194, 19–37. doi:10.1016/j.earscirev.2019.04.026

Medwedeff, D. A., and Suppe, J. (1997). Multi Bend Fault-Bend Folding. *J. Struct. Geol.* 19, 279–292. doi:10.1016/s0191-8141(97)83026-x

Peng, S. (1995). Active Tectonics and Earthquake Hazards of the Turfan Basin. Northwestern China Beijing: Institute of Geology, China Earthquake Administration dissertation 's thesis [in Chinese with English abstract].

Ren, G., Li, C., Wu, C., Wang, S., Zhang, H., Ren, Z., et al. (2019). The Late Quaternary Activity and Formation Mechanism of Baoertu Fault Zone, Eastern Tianshan Segment. *Seismology Geology.* 41, 856–871. [in Chinese with English Abstract]. doi:10.3969/j.issn.0253-4967.2019.04.004

Saint-Carlier, D., Charreau, J., Lavé, J., Blard, P. H., Dominguez, S., Avouac, J. P., et al. (2016). Major Temporal Variations in Shortening Rate Absorbed along a Large Active Fold of the Southeastern Tianshan Piedmont (China). *Earth Planet. Sci. Lett.* 434, 333–348. doi:10.1016/j.epsl.2015.11.041

Scharer, K. M., Burbank, D. W., Chen, J., and Weldon, R. J. (2006). Kinematic Models of Fluvial Terraces over Active Detachment Folds: Constraints on the Growth Mechanism of the Kashi-Atushi Fold System, Chinese Tian Shan. *Geol. Soc. Am. Bull.* 118, 1006–1021. doi:10.1130/B25835.1

Shen, J., Wang, Y., Li, Y., Jiang, H., and Xiang, Z. (2003). Late Quaternary Right Lateral Strike-Slip Faulting along the Bolokenu-Aqikekuduke Fault in Chinese Tian Shan. *Seismology Geology.* 25, 183–194. [in Chinese with English abstract]. doi:10.3969/j.issn.0253-4967.2003.02.002

Stockmeyer, J. M., Shaw, J. H., Brown, N. D., Rhodes, E. J., Richardson, P. W., Wang, M., et al. (2017). Active Thrust Sheet Deformation over Multiple Rupture Cycles: A Quantitative Basis for Relating Terrace Folds to Fault Slip Rates. *GSA Bull.* 129, 1337–1356. doi:10.1130/B31590.1

Storti, F., and Poblet, J. (1997). Growth Stratal Architectures Associated to Decollement Folds and Fault-Propagation Folds. Inferences on Fold Kinematics. *Tectonophysics* 282, 353–373. doi:10.1016/S0040-1951(97)00230-8

Suppe, J., Chou, G. T., and Hook, S. C. (1992). "Rates of Folding and Faulting Determined from Growth Strata," in *"Thrust Tectonics*. Editor K. R. McClay (London, UK: Chapman and Hall), 105–121.

Suppe, J. (1983). Geometry and Kinematics of Fault-Bend Folding. *Am. J. Sci.* 283, 684–721. doi:10.2475/ajs.283.7.684

Suppe, J., Sabat, F., Munoz, J. A., Poblet, J., and Verges, J. (1997). Bed-by-bed Fold Growth by Kink-Band Migration: Sant Llorencde Morunys, Eastern Pyrenee. *J. Struct. Geology.* 19, 443–461. doi:10.1016/S0191-8141(96)00103-4

Tapponnier, P., and Molnar, P. (1979). Active Faulting and Cenozoic Tectonics of the Tien Shan, Mongolia, and Baykal Regions. *J. Geophys. Res.* 84, 3425–3459.

Thompson, S. C., Weldon, R. J., Rubin, C. M., Abdrakhmatov, K., Molnar, P., and Berger, G. W. (2002). Late Quaternary Slip Rates across the Central Tien Shan, Kyrgyzstan, Central Asia. *J. Geophys. Res.* 107, 2203. doi:10.1029/2001JB000596

Trexler, C. C., Cowgill, E., Spencer, J. Q. G., and Godoladze, T. (2020). Rate of Active Shortening across the Southern Thrust Front of the Greater Caucasus in Western georgia from Kinematic Modeling of Folded River Terraces above a Listric Thrust. *Earth Planet. Sci. Lett.* 544, 116362. doi:10.1016/j.epsl.2020.116362

Wang, M., and Shen, Z. K. (2020). Present-day Crustal Deformation of Continental China Derived from GPS and its Tectonic Implications. *J. Geophys. Res.* 125, e2019JB018774. doi:10.1029/2019JB018774

Wang, S., Jiao, R., Ren, Z., Wu, C., Ren, G., Zhang, H., et al. (2020a). Active Thrusting in an Intermontane Basin: The Kumysh Fault, Eastern Tian Shan. *Tectonics* 39, e2019TC006029. doi:10.1029/2019TC006029

Wang, Y., Oskin, M. E., Zhang, H., Li, Y., Hu, X., and Lei, J. (2020b). Deducing Crustal-scale Reverse-fault Geometry and Slip Distribution from Folded River Terraces, Qilian Shan, China. *Tectonics* 39, e2019TC005901. doi:10.1029/2019TC005901

Wu, C., Wu, G., Shen, J., Dai, X., Chen, J., and Song, H. (2016). Late Quaternary Tectonic Activity and Crustal Shortening Rate of the Bogda Mountain Area, Eastern Tian Shan, China. *J. Asian Earth Sci.* 119, 20–29. doi:10.1016/j.jseaes.2016.01.001

Wu, G., Yao, T., Thompson, L. G., and Li, Z. (2004). Microparticle Record in the Guliya Ice Core and its Comparison with Polar Records since the Last Interglacial. *Chin. Sci. Bull.* 49, 607–611. doi:10.1360/03wd0419

Yang, S. M., Li, J., and Wang, Q. (2008). The Deformation Pattern and Fault Rate in the Tianshan Mountains Inferred from GPS Observations. *Sci. China. Ser. D: Earth Sci.* 51, 1064–1080. doi:10.1007/s11430-008-0090-8

Yao, H., Li, W., and Wang, G. (2013). Oil and Gas Characteristics of Thrusting-Nappe Structure Belt in Huoyanshan, Xinjiang. *J. Geomechanics* 19, 206–213. [in Chinese with English Abstract]. doi:10.3969/j.issn.1006-6616.2013.02.010

Yin, A., Nie, S., Craig, P., Harrison, T. M., Ryerson, F. J., Qian, X., et al. (1998). Late Cenozoic Tectonic Evolution of Southern Chinese Tianshan. *Tectonics* 17, 1–27. doi:10.1029/97TC03140

Zhang, P. Z., Shen, Z. K., Min, W., Gan, W. J., and Burgmann, R. (2004). Continuous Deformation of the Tibetan Plateau from Global Positioning System Data. *Geology* 32, 809–812. doi:10.1130/G20554.1

Zubovich, A. V., Wang, X. Q., Scherba, Y. G., Schelochkov, G. G., Reilinger, R., Reigber, C., et al. (2010). GPS Velocity Field for the Tien Shan and Surrounding Regions. *Tectonics* 29, TC6014. doi:10.1029/2010TC002772

Conflict of Interest: The authors declare that the research was conducted in the absence of any commercial or financial relationships that could be construed as a potential conflict of interest.